Supplementary information

To

Bulk substitution of F-terminations from $Ti_3C_2T_x$ MXene by cation pillaring and gas hydrolysation

Frode Håskjold Fagerli,[a] Per Erik Vullum,[bc] Tor Grande,[a] Zhaohui Wang,[ab] Sverre M. Selbach,[a] Kjell Wiik[a] and Nils Peter Wagner[ab*]

a. Department of Materials Science and Engineering, Norwegian University of Science and Technology, NO-7034 Trondheim, Norway.
b. SINTEF Industry, NO-7034 Trondheim, Norway.
c. Department of Physics, Norwegian University of Science and Technology, NO-7034 Trondheim, Norway.

* nils.peter.wagner@sintef.no

Additional Figures and Tables

The Figures included here present:

The Tables included here present:

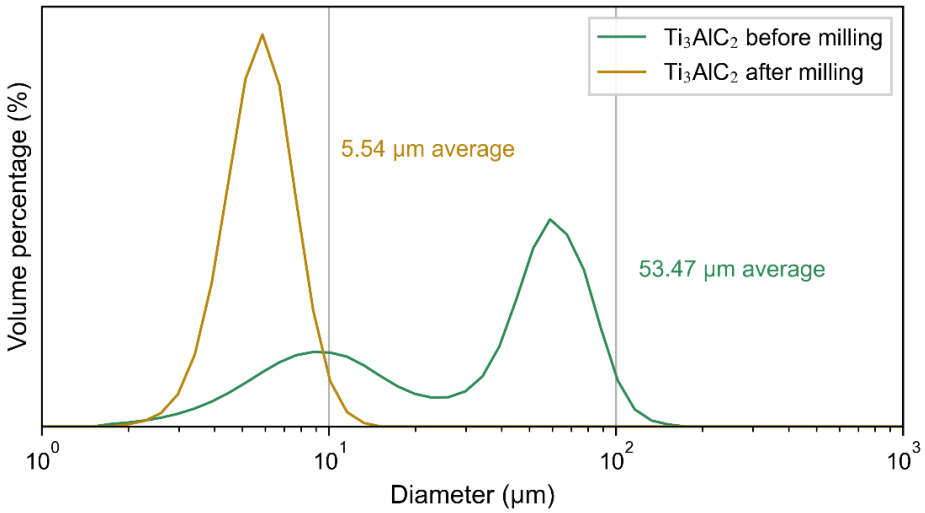

Figure S1. Particle size distribution of the Ti_3AlC_2 MAX phase before and after wet milling for 150 min in isopropanol.

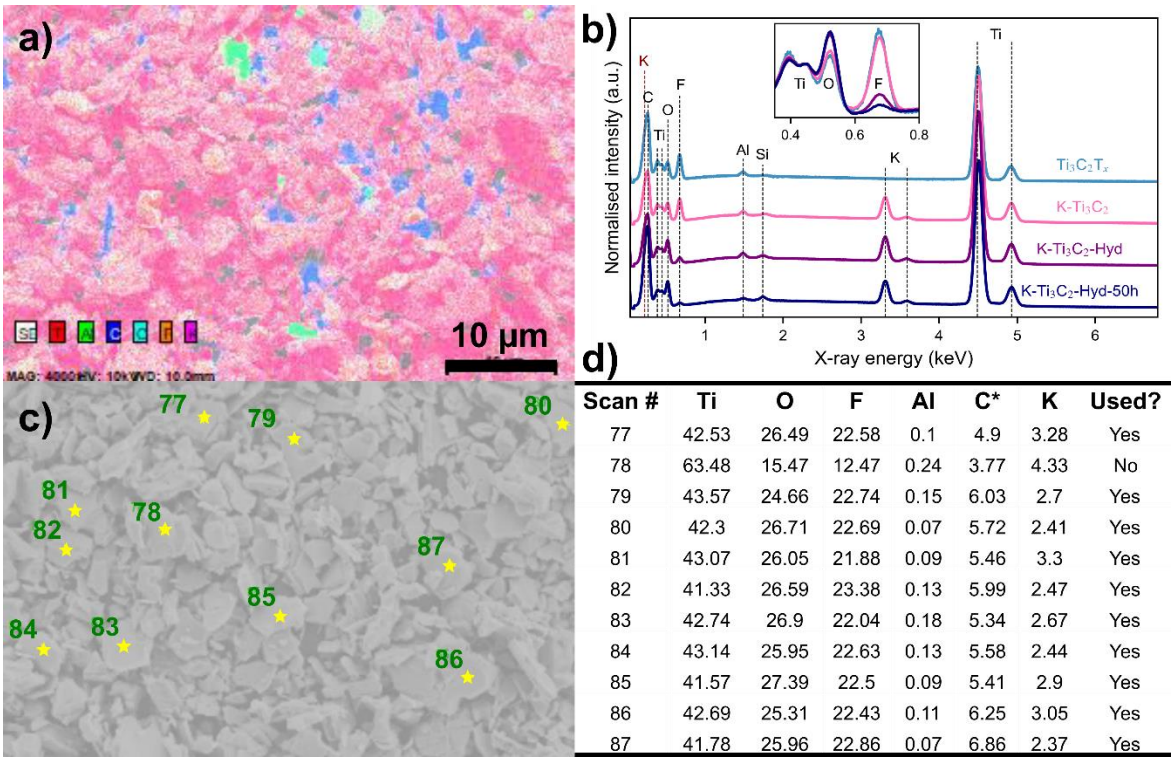

d)

Scan #	Ti	O	F	Al	C*	K	Used?
77	42.53	26.49	22.58	0.1	4.9	3.28	Yes
78	63.48	15.47	12.47	0.24	3.77	4.33	No
79	43.57	24.66	22.74	0.15	6.03	2.7	Yes
80	42.3	26.71	22.69	0.07	5.72	2.41	Yes
81	43.07	26.05	21.88	0.09	5.46	3.3	Yes
82	41.33	26.59	23.38	0.13	5.99	2.47	Yes
83	42.74	26.9	22.04	0.18	5.34	2.67	Yes
84	43.14	25.95	22.63	0.13	5.58	2.44	Yes
85	41.57	27.39	22.5	0.09	5.41	2.9	Yes
86	42.69	25.31	22.43	0.11	6.25	3.05	Yes
87	41.78	25.96	22.86	0.07	6.86	2.37	Yes

Figure S2. EDS results together with an example of how the point scan averages in Table S1 were obtained. (a) shows EDS mapping of the K-Ti_3C_2 sample, (c) shows the selected point scans from the same area, (d) shows the atomic percentages obtained from the analysis of the point scans in (c), and (b) shows a comparison of the normalised EDS mapping spectra for the hydrolysation of K-intercalated $Ti_3C_2T_x$. The inset in (b) displays a comparison of the O and F peaks after normalising the plots to the Ti peaks, demonstrating a significant reduction of the F peak upon hydrolysation. As stated in (d), one spectrum (78) was omitted for the calculation of the average values for K-Ti_3C_2. It was omitted as the analysis software could not adjust for the high tilt, which thus resulted in an increase in the high energy components (i.e. Ti and K) versus the low energy components (i.e. O and F). The X-ray energies for the different atoms in (b) were collected from the Esprit 1.9 software, and as illustrated by the overlap of the K and C peak at ~0.26 kV, the calculated C content in (d) was perturbed.

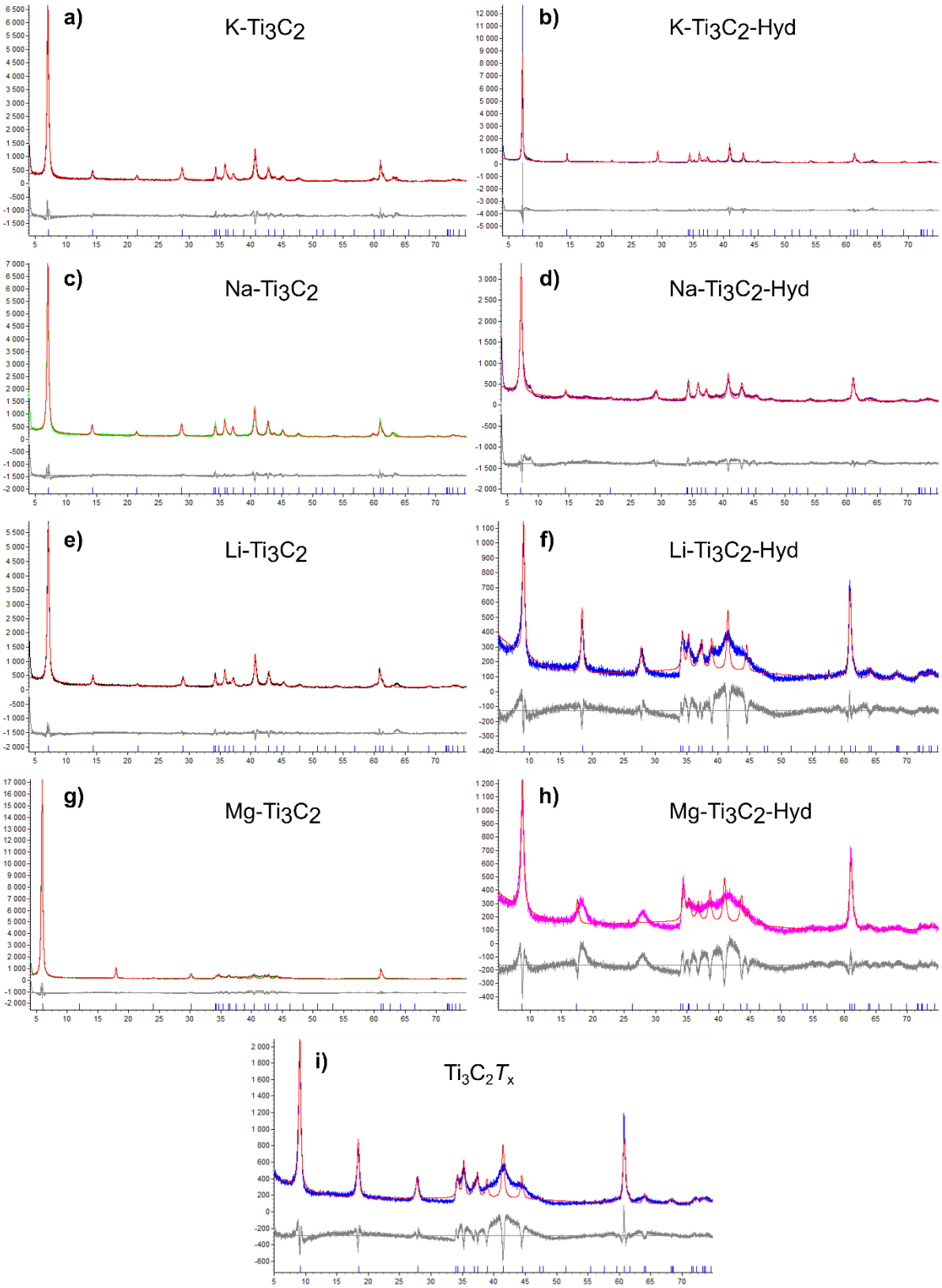

Figure S3. Pawley fitting of X-ray diffractograms for pristine $Ti_3C_2T_x$ *MXene before (i) and after the intercalation of the various cations (a,c,e,g), followed by hydrolysation at 300 ˚C (b,d,f,h), illustrating how well the fitting matched with the experimentally obtained diffractograms. The non-intercalated samples (*$Ti_3C_2T_x$*,* Li-Ti_3C_2-Hyd *and* Mg-Ti_3C_2-Hyd*) show a higher degree of stacking faults, as they result in stronger fitting mismatches in the 35-45˚ 2θ region.*[1]

Table S1. Overview over the EDS point scan averages and standard deviations that are used in this article. The amounts are presented relative to one formula unit of $Ti_3C_2T_x$ (or a Ti amount of 3). The C quantification of K-Ti_3C_2 is disturbed by the K and C X-rays overlapping (Figure S2b), and Li is not detectable in EDS. The results above the vertical midline represent annealing of pristine HF-etched $Ti_3C_2T_x$, where the name indicates what atmosphere and temperature is used. Below the midline are the results from the intercalation of cations into $Ti_3C_2T_x$ followed by hydrolysation at 300 ˚C.

Sample	Ti	Al	C	O	F	Mg/Na/K
Ti_3AlC_2	3 ± 0.14	1.00 ± 0.05	1.97 ± 0.13			
Ti_3C_2	3 ± 0.34	0.01 ± 0.01	1.57 ± 0.14	1.35 ± 0.11	1.39 ± 0.12	
Hyd300C	3 ± 0.19	0.01 ± 0.00	1.59 ± 0.05	1.42 ± 0.15	1.36 ± 0.07	
Hyd400C	3 ± 0.24	0.01 ± 0.00	1.85 ± 0.24	1.97 ± 0.13	1.21 ± 0.14	
Hyd450C	3 ± 0.15	0.01 ± 0.00	1.54 ± 0.11	2.09 ± 0.35	1.18 ± 0.18	
Hyd500C	3 ± 0.12	0.01 ± 0.01	1.38 ± 0.03	6.09 ± 0.26	0.09 ± 0.13	
Vac500C	3 ± 0.15	0.01 ± 0.00	1.61 ± 0.12	1.45 ± 0.08	1.33 ± 0.08	
Ar500C	3 ± 0.10	0.01 ± 0.00	1.65 ± 0.04	1.51 ± 0.08	1.43 ± 0.05	
H_2/Ar-500C	3 ± 0.17	0.01 ± 0.00	1.75 ± 0.14	1.30 ± 0.08	1.35 ± 0.06	
Air300C	3 ± 0.24	0.01 ± 0.00	1.45 ± 0.12	2.43 ± 0.36	1.29 ± 0.22	
Air400C	3 ± 0.26	0.01 ± 0.00	0.40 ± 0.37	5.44 ± 0.33	0.39 ± 0.17	
Air500C	3 ± 0.09	0.01 ± 0.00	0.36 ± 0.18	5.67 ± 0.23	0.33 ± 0.16	
TBA-Ti_3C_2	3 ± 0.07	0.00 ± 0.00	2.77 ± 0.15	1.41 ± 0.08	1.22 ± 0.06	
TBA-Ti_3C_2-Hyd	3 ± 0.13	0.01 ± 0.01	1.77 ± 0.10	1.87 ± 0.18	0.99 ± 0.08	
K-Ti_3C_2	3 ± 0.05	0.01 ± 0.00	0.41 ± 0.04	1.85 ± 0.06	1.59 ± 0.03	0.19 ± 0.03
K-Ti_3C_2-Hyd	3 ± 0.10	0.01 ± 0.00	0.44 ± 0.02	2.61 ± 0.11	0.51 ± 0.09	0.21 ± 0.04
K-Ti_3C_2-Hyd-50h	3 ± 0.22	0.01 ± 0.01	0.47 ± 0.03	2.82 ± 0.22	0.31 ± 0.07	0.23 ± 0.02
K-Ti_3C_2-Ar300C	3 ± 0.15	0.01 ± 0.00	0.00 ± 0.02	2.47 ± 0.15	1.22 ± 0.15	0.23 ± 0.01
Mg-Ti_3C_2*	3 ± 0.25	0.01 ± 0.00	1.79 ± 0.14	2.24 ± 0.14	1.06 ± 0.24	0.18 ± 0.01
Mg-Ti_3C_2-Hyd*	3 ± 0.28	0.01 ± 0.01	1.95 ± 0.39	2.10 ± 0.28	1.12 ± 0.21	0.18 ± 0.03
Na-Ti_3C_2	3 ± 0.17	0.01 ± 0.01	1.47 ± 0.08	1.41 ± 0.08	1.13 ± 0.04	0.21 ± 0.07
Na-Ti_3C_2-Hyd	3 ± 0.13	0.01 ± 0.00	1.40 ± 0.07	1.80 ± 0.29	0.77 ± 0.23	0.16 ± 0.01
Li-Ti_3C_2	3 ± 0.18	0.01 ± 0.00	1.58 ± 0.10	1.62 ± 0.10	1.36 ± 0.06	
Li-Ti_3C_2-Hyd	3 ± 0.13	0.01 ± 0.00	1.61 ± 0.07	1.58 ± 0.13	1.28 ± 0.08	

- No Cl peaks were detected in the Mg-Ti_3C_2 samples.

Table S2. Comparison between the chemical quantifications obtained from EDS mapping and point scans for all MXene compositions presented in this article, where the F content is highlighted with colour coding to emphasize the changes (green = low, and red = high). Apart from the unstable C content in the mapping, which is a result of extra signal from the C tape background, there are similar tendencies for both the mapping and point scan results. The amounts are presented relative to one formula unit of $Ti_3C_2T_x$ (or a Ti amount of 3). The cations are Mg, Na or K, although Al content is shown for Ti_3AlC_2 MAX phase before and after etching. Noteworthy, seeing that the EDS mapping results show similar trends as the point scan averages, the use of EDS mapping may prove to be sufficient for rough quantification of O and F content for MXenes, if the number of impurity particles in the mapped regions are consistent.

	Mapping				Point scans			
Sample	**C**	**O**	**F**	**Cation**	**C**	**O**	**F**	**Cation**
Ti_3AlC_2	2.22			1.00 (Al)	1.97			1.00 (Al)
Ti_3C_2	3.58	1.81	1.56	0.03 (Al)	1.57	1.35	1.39	0.01 (Al)
Hyd300C	2.81	1.87	1.52		1.59	1.42	1.36	
Hyd400C	3.79	2.50	1.20		1.85	1.97	1.21	
Hyd450C	2.36	2.74	1.13		1.54	2.09	1.18	
Hyd500C	1.99	6.78	0.06		1.38	6.09	0.09	
Vac500C	3.72	2.01	1.53		1.61	1.45	1.33	
Ar500C	2.79	1.93	1.39		1.65	1.51	1.43	
H_2/Ar500C	3.11	1.76	1.53		1.75	1.30	1.35	
Air300C	2.06	2.97	1.16		1.45	2.43	1.29	
Air400C	1.85	5.85	0.44		0.40	5.44	0.39	
Air500C	1.42	6.37	0.22		0.36	5.67	0.33	
TBA-Ti_3C_2	2.80	1.58	1.26		2.77	1.41	1.22	
TBA-Ti_3C_2-Hyd	1.53	1.57	0.71		1.77	1.87	0.99	
K-Ti_3C_2	0.47	1.75	1.27	0.23	0.41	1.85	1.59	0.19
K-Ti_3C_2-Hyd	0.44	2.17	0.38	0.24	0.44	2.61	0.51	0.21
K-Ti_3C_2-Hyd-50h	0.87	2.51	0.24	0.22	0.47	2.82	0.31	0.23
K-Ti_3C_2-Ar300C	0.00	2.51	1.13	0.23	0.00	2.47	1.22	0.23
Mg-Ti_3C_2	3.06	2.13	0.99	0.18	1.79	2.24	1.06	0.18
Mg-Ti_3C_2-Hyd	8.91	2.74	0.96	0.16	1.95	2.10	1.12	0.18
Na-Ti_3C_2	2.91	2.08	1.55	0.39	1.47	1.41	1.13	0.21
Na-Ti_3C_2-Hyd	3.55	2.47	0.78	0.25	1.40	1.80	0.77	0.16
Li-Ti_3C_2	2.06	1.97	1.48		1.58	1.62	1.36	
Li-Ti_3C_2-Hyd	7.07	2.34	1.32		1.61	1.58	1.28	

Synthesis of $Ti_3C_2T_x$ MXene

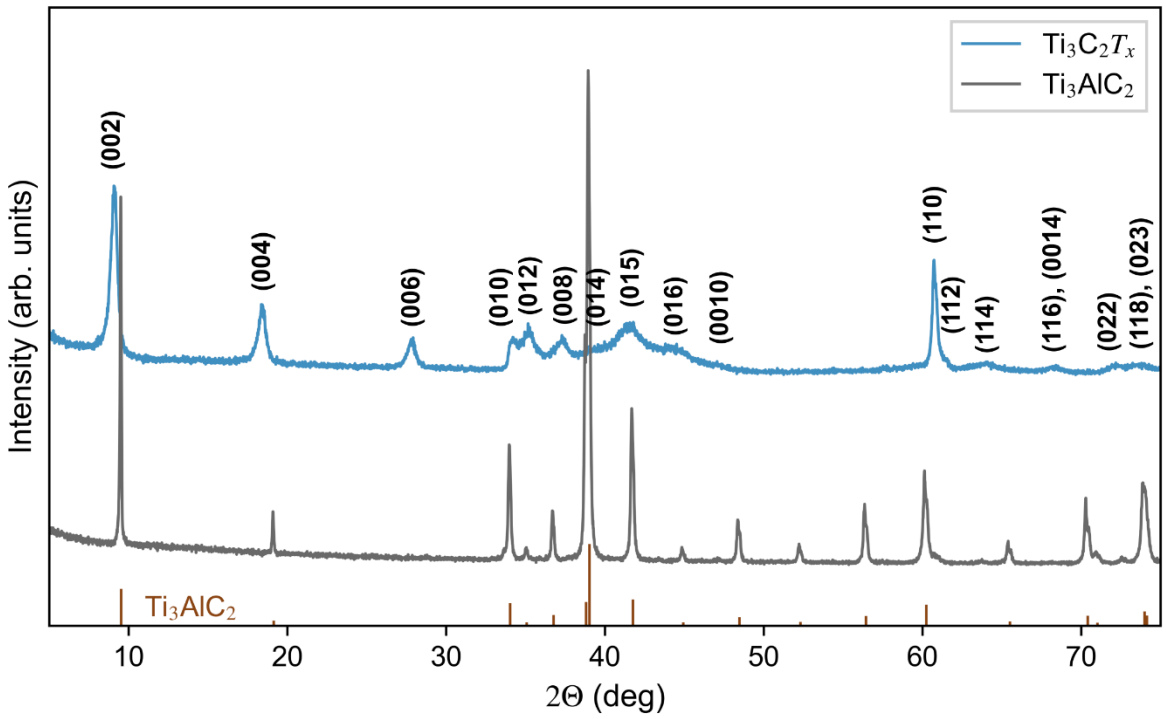

Figure S4. X-ray diffractograms before and after etching of the Ti_3AlC_2 *MAX phase in 10 wt. %* HF. *As there are no reflections left from the MAX phase, it is assumed 100 % etching of the* Al *layer to form pure* $Ti_3C_2T_x$ *MXene. The theoretical* Ti_3AlC_2 *reflections are obtained from PDF 04-012-0632, and the marked (hkl) reflections of the MXene is obtained from the structureless Pawley fitting using the* $P6_3/mmc$ *space group.*

Gas hydrolysation of pristine HF-etched $Ti_3C_2T_x$ MXene

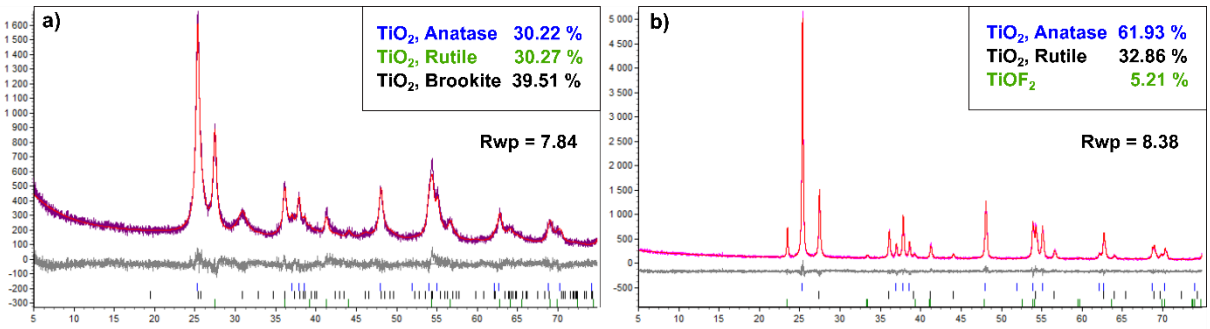

Figure S5. Rietveld refinement of the X-ray diffractograms from $Ti_3C_2T_x$ *after hydrolysation (a) and air annealing (b) at 500 ˚C. It shows the estimated amounts of the different phases present after oxidation of the* $Ti_3C_2T_x$ *phase.*

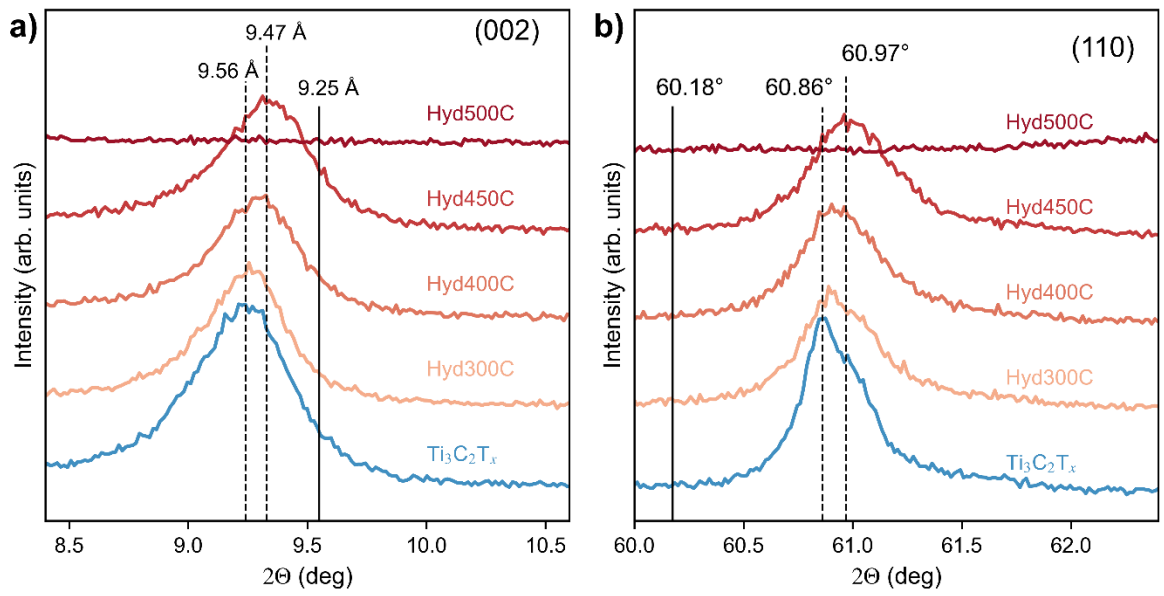

Figure S6. Specific regions from the X-ray diffractograms presented in Figure 2a indicating the shifts in the (002) reflection which gives the interlayer spacing of the $Ti_3C_2T_x$ *MXene (a) and the (110) reflection which may describe changes in stacking of the MXene layers (b). The dashed lines indicate the positions of the* reflections *before and after hydrolysation at 450 ˚C, while the solid line represent positions of the same reflections for the* Ti_3AlC_2 *MAX phase. These plots are adjusted for sample displacement through a structureless fitting with the* $P6_3/mmc$ *space group.*

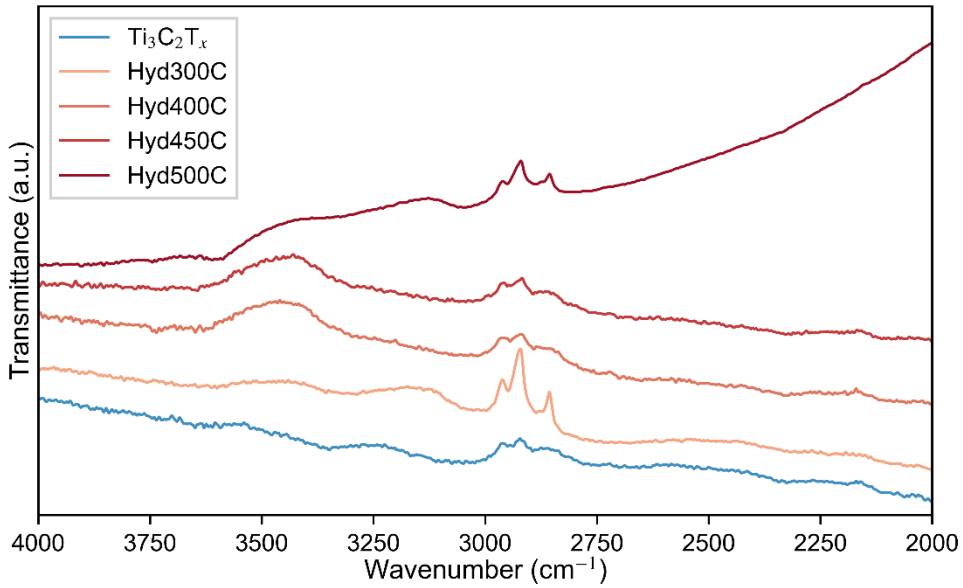

Figure S7. Extended region of the FTIR spectra presented in Figure 2c, where there are no significant transmission valleys (absorption peaks) visible in the H_2O *region around 3000* cm^{-1} *to 3600* cm^{-1}*. Instead, transmission peaks are observed, indicating that there are some problems with the* KBr *reference, as the reference material may contain more water than the MXene particles. The transmission peaks at around 2900* cm^{-1} *come from* sp^3 C-H *stretching modes which come from impurities in the instrument used.*

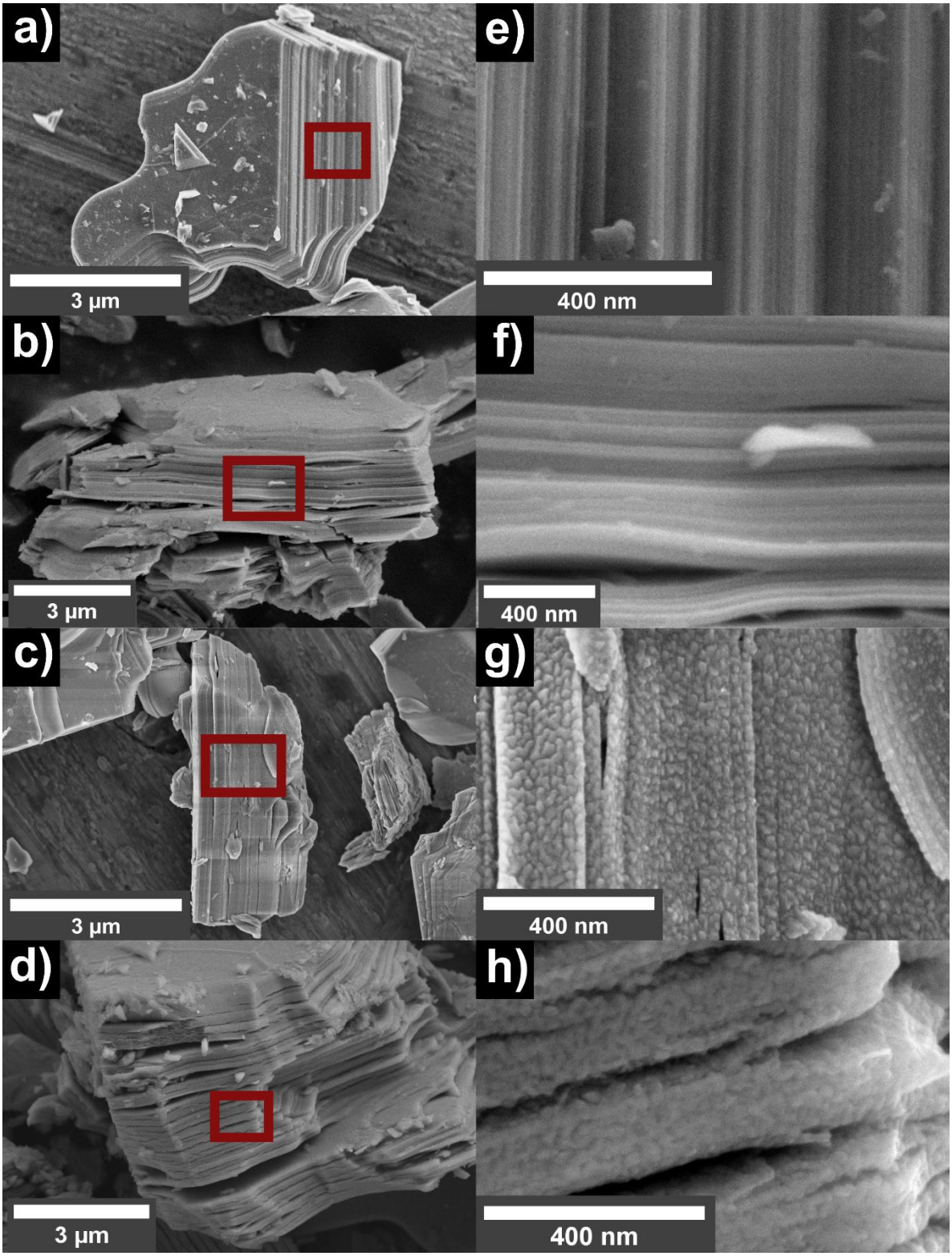

Figure S8. SEM micrographs depicting the morphology of the $Ti_3C_2T_x$ *particles at low (a-d) and high (e-h) magnification, both before (a,e) and after hydrolysation at 300 ˚C (b,f), 400 ˚C (c,g) and 500 ˚C (d,h). It shows the formation of nanoparticles on the edge surface after hydrolysation at temperatures above 300 ˚C.*

Characterisation of local chemical compositional changes at the edge surface

To investigate if there were any local compositional changes within the $Ti_3C_2T_x$ particles after the hydrolysation, TEM EDS mapping was performed on the particle edges before and after hydrolysation at 400 ˚C. The results are presented in Figure S9, showing the variation in concentration of Ti, C, O and F along a cross section of the particles. Apart from the C increase at the edge of the particle, deriving from the carbon protection layer deposited inside the FIB during TEM preparation, all other concentrations diminish outside the particle. After hydrolysation at 400 ˚C, the formation of TiO_2 nanoparticles is seen as a peak in the O content at the particle surface. However, as the ratio between O and F terminations remain unchanged before and after hydrolysation, and within the particles, it is concluded that the gas hydrolysation of pristine HF-etched $Ti_3C_2T_x$ does not result in any substitution of F-terminations.

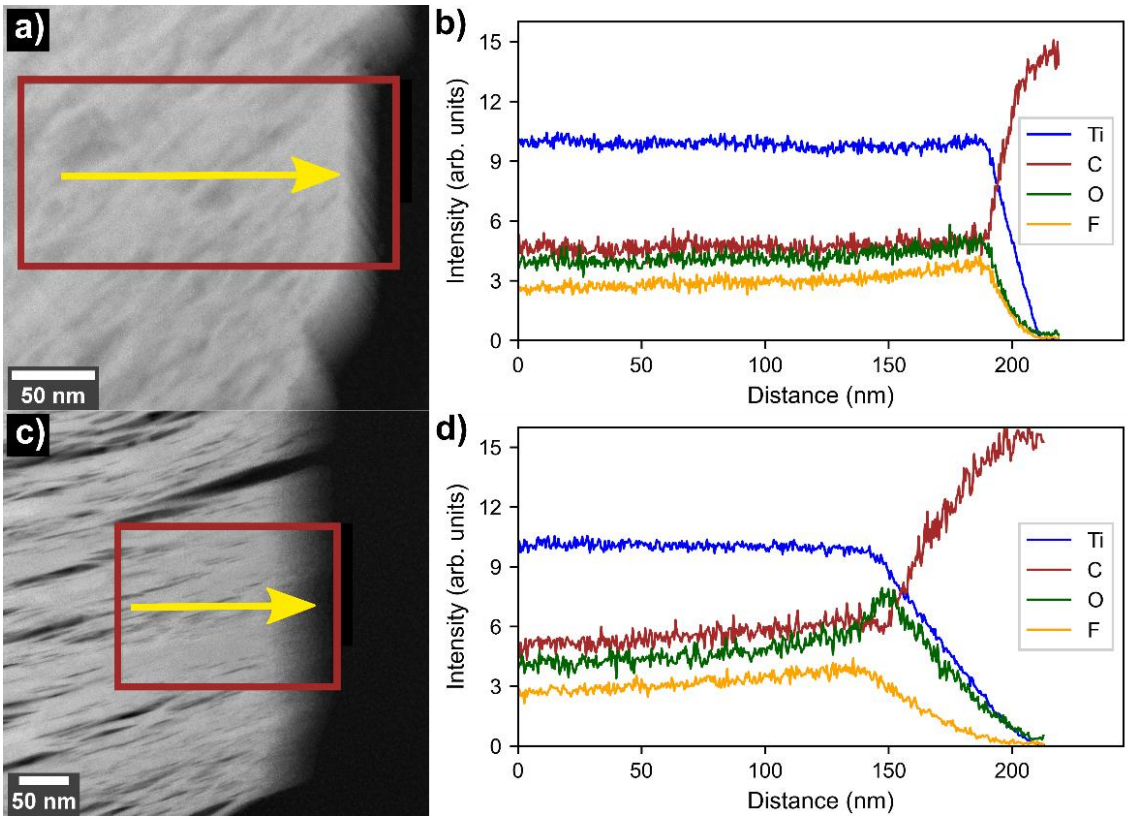

Figure S9. STEM EDS mapping of regions that include the edge surface of $Ti_3C_2T_x$ *particles before (a,b) and after (c,d) hydrolysation at 400 ˚C. a) and c) are HAADF-STEM images where the red frames illustrate the mapped regions, while b) and d) demonstrate the intensities of* Ti, C, O *and* F *as a function of the distance from left to right in the red areas depicted in a) and c).*

Comparing the thermal stability of pristine $Ti_3C_2T_x$ in various atmospheres

To compare the thermal stability of $Ti_3C_2T_x$ in humid atmosphere to other atmospheres, $Ti_3C_2T_x$ was annealed in inert (Ar), reducing (H_2/Ar) and oxidising (synthetic air) atmospheres as well as under vacuum. For annealing in air (Figure S10), it is shown that the oxidation starts at a lower temperature than for hydrolysis (300 ˚C compared to 400 ˚C) and that the MXene phase is completely oxidised to TiO_2 anatase and rutile phases after annealing at 400 ˚C (Figure S10 a and b). The Raman and EDS results also demonstrate how the oxidation in air drastically reduces the C content by more than 80 % (Figure S10 b and c). Comparing this to hydrolysation, where most of the C remained even after complete oxidation at 500 ˚C, a faster oxidation of C in the presence of O_2 gas is demonstrated. Additionally, the oxidation in air resulted in the formation of larger crystallites and did not preserve the layered morphology of the particles (Figure S11). Considering the F content upon annealing in dry air, there is a significant reduction following the oxidation of the MXene phase. However, as almost 25 % of the initial F content remains as a $TiOF_2$ phase even after annealing at 500 ˚C (Figure S5b and Table S1), air annealing demonstrates an inferior selectivity towards F removal compared to hydrolysation, where almost 100 % of the F content was removed. As similar results are reported for the oxidation in pure O_2,[2] and seeing that the MXene oxidation by O_2 is accompanied by a high thermodynamic driving force (Figure S12),[3] annealing in oxygen is not a good alternative for F-termination substitution.

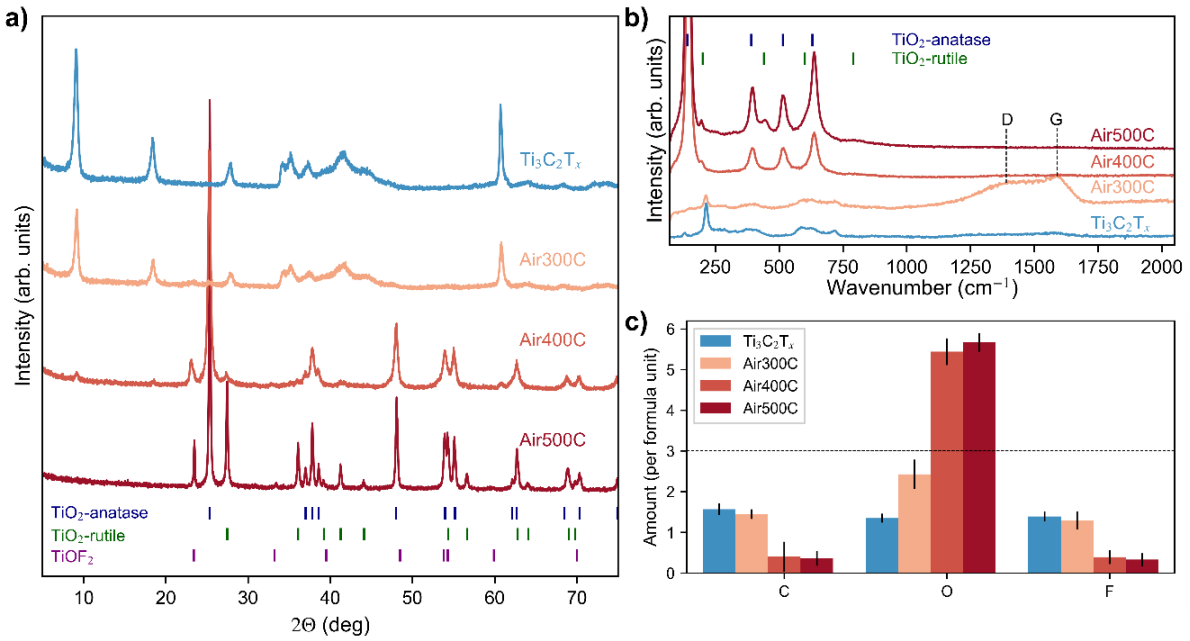

Figure S10. Results from the annealing of $Ti_3C_2T_x$ in synthetic air at different temperatures showing X-ray diffractograms (a), Raman spectra (b) and EDS average values (c). The dashed line in (c) illustrates a Ti *amount of 3 and the error bars represent the standard deviation from the set of point scans used for each sample.*

X-ray diffractograms, FTIR spectra and EDS quantification results from annealing of $Ti_3C_2T_x$ in inert, reducing, oxidising and vacuum environments are presented in the supplementary information (Table S1, Figure S13 and S14) and demonstrate the differences after annealing at 500 ˚C. As previously discussed, both the hydrolysation and air annealing of $Ti_3C_2T_x$ resulted in a complete oxidation at this temperature. However, whereas the hydrolysation preserved the C content while removing all F content, the air annealed $Ti_3C_2T_x$ shows a Ti-F shoulder at 951 cm^{-1} in the FTIR spectra and none of the C-related vibrational modes. For the MXene annealed under vacuum, inert and reducing atmospheres, only minor changes are observed. Although the XRD and FTIR results demonstrate slight decomposition into TiO_2 and C or TiF_3 phases at this temperature (Figure S13 and S14), the chemical composition of these samples remained the same (Table S1). Considering possible reaction products from F-removal, such as HF (g), F_2 (g), CF_4 (g) and F^-, HF gas would be the most likely product to leave the structure without damaging the MXene. While evaporation of F^- ions would result in a build-up of positive charge on the MXene, oxidation into F_2 gas is unattainable due to the high reduction potential of F. Additionally, the formation of carbon fluorides would depend on the decomposition of the MXene phase in order to have the required C content. Seeing that reactions with H_2O may allow for the formation of HF gas (Figure 1), a humid atmosphere (hydrolysation) is therefore expected to be the ideal annealing atmosphere for removal of F-terminations from MXenes.

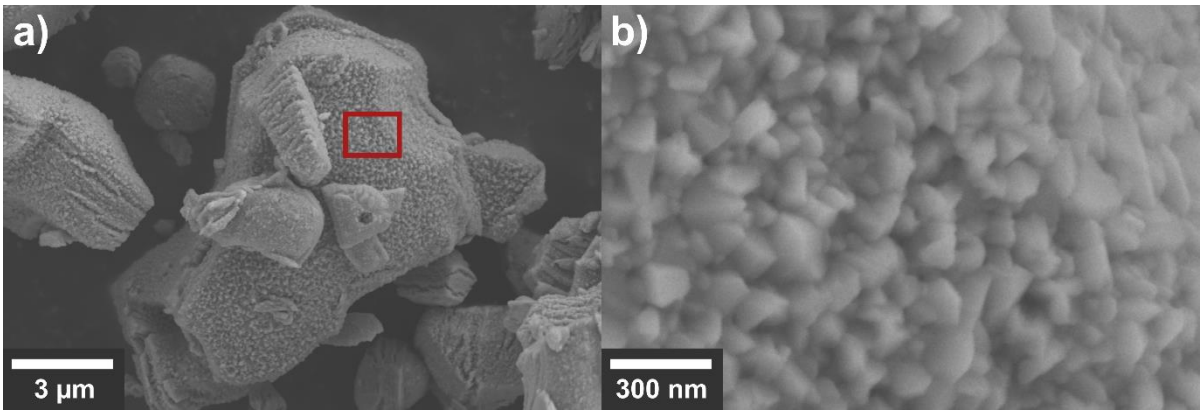

Figure S11. Low and high magnification SEM micrographs of $Ti_3C_2T_x$ *particles after annealing in dry air at 500 ˚C, where (b) represents the region marked in red in (a).*

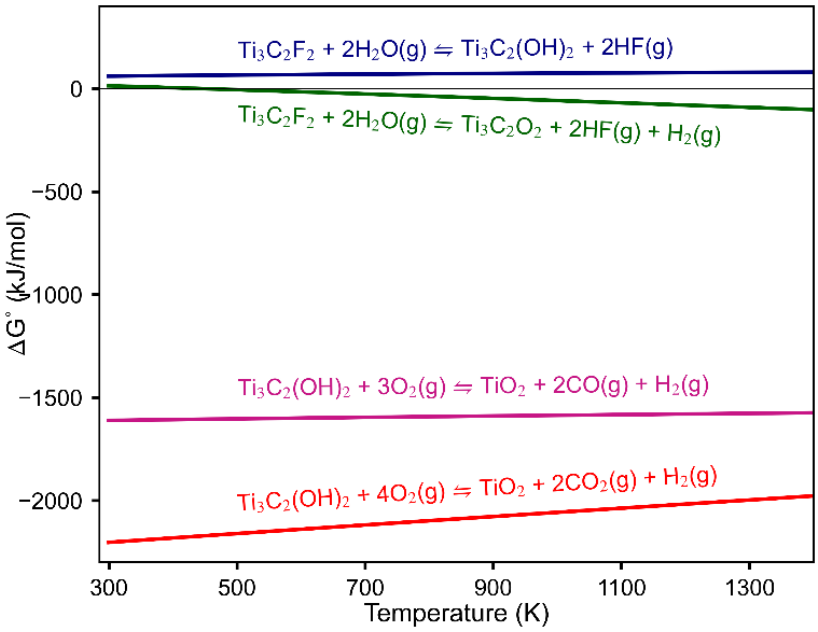

Figure S12. DFT results from four reactions showing ΔG˚ as a function of temperature. It demonstrates how the oxidation of $Ti_3C_2(OH)_2$ *is very thermodynamically favourable in* O_2 *atmosphere.*

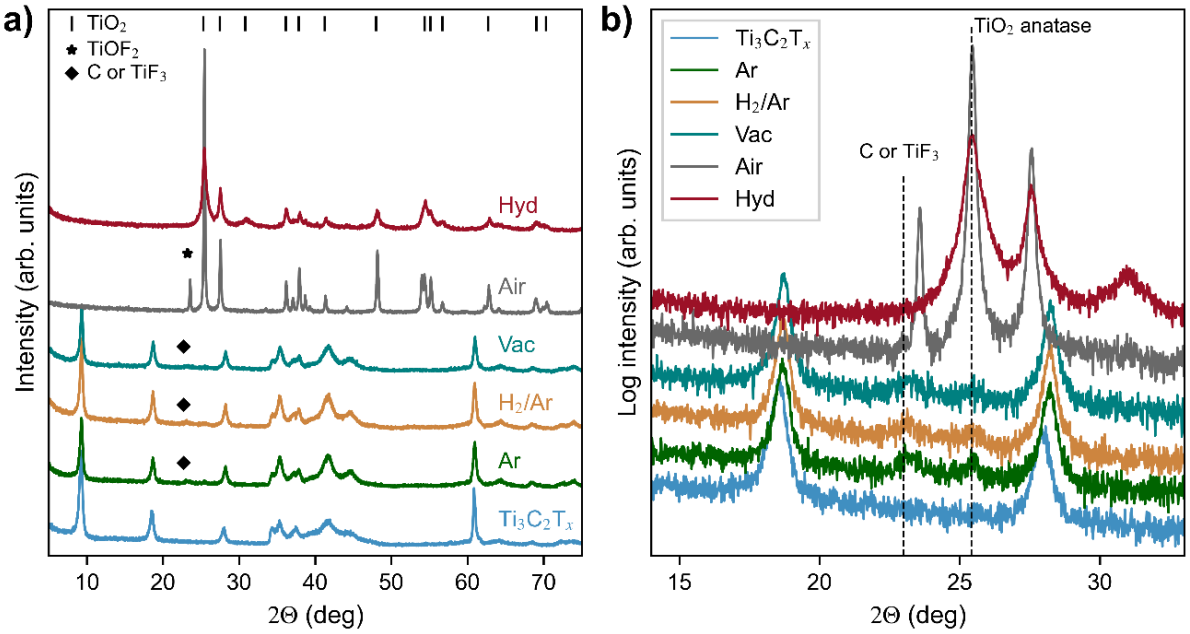

Figure S13. X-ray diffractograms of $Ti_3C_2T_x$ *before and after annealing for 15 h at 500 ˚C in various atmospheres. (a) shows the overall spectra, whereas (b) shows logarithmic intensities from a smaller 2θ region. The names of the different samples indicate what atmospheres are used, where "Vac" represents vacuum and "Hyd" represent hydrolysis.*

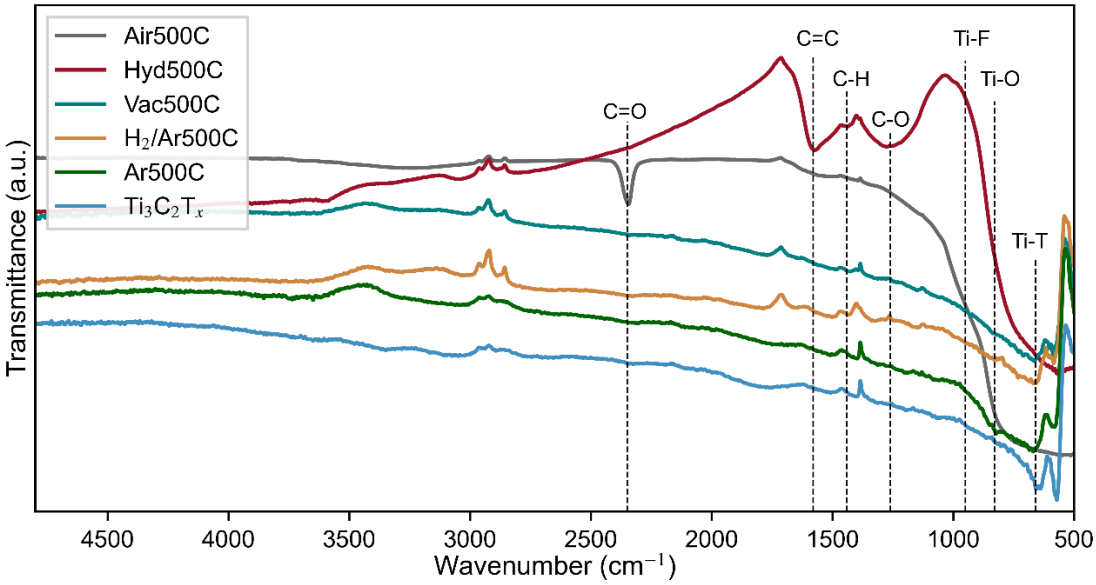

Figure S14. FTIR spectra of $Ti_3C_2T_x$ *before and after annealing at 500 ˚C in various atmospheres, where the names indicate which atmospheres are used. The marked transmission valleys represent the vibrations of the* C=O *stretching mode from* CO_2 *at 2351* cm^{-1}*, the* C=C *stretching mode at 1577* cm^{-1}*, the* C-H *bending mode at 1439* cm^{-1}*, the* C-O *stretching mode at 2354* cm^{-1}*, the* Ti-F *mode from the* $TiOF_2$ *phase at 951* cm^{-1}*,*[4] *the* Ti-O *mode from anatase with its edge starting at around 800* cm^{-1}*,*[5] *and the ascribed* Ti-*T bond between MXene* Ti *atoms and surface terminations T at ~660* cm^{-1}*. The peaks (not valleys) presented in these plots come from instrument impurities and/or impurities in the reference. The presence of* CO_2 *in the Air annealed sample may come from trapped* CO_2 *inside the particles.*

Hydrolysation of pre-intercalated $Ti_3C_2T_x$

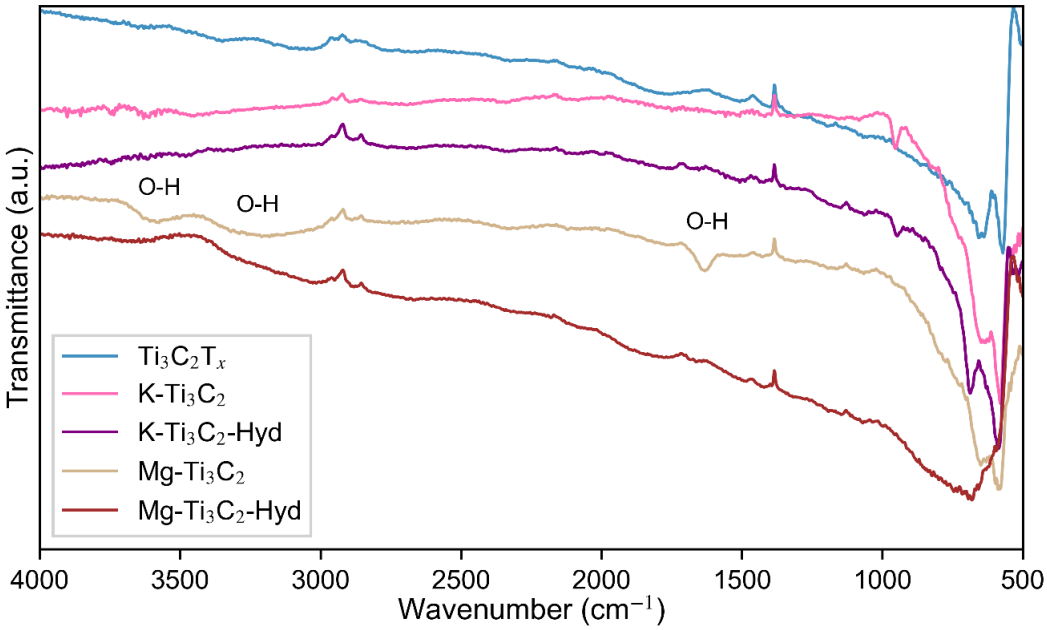

Figure S15. FTIR spectra of $Ti_3C_2T_x$ *samples with the intercalation of* K- *and* Mg-*ions before and after hydrolysation at 300 ˚C for 15 h. The* O-H *bending (1650* cm^{-1}*) and stretching modes (~3300* cm^{-1} *and 3600* cm^{-1}*) indicative of water molecules are only present for the* Mg-*intercalated* $Ti_3C_2T_x$*. The peaks (not valleys) presented in these plots come from instrument impurities and/or impurities in the reference.*

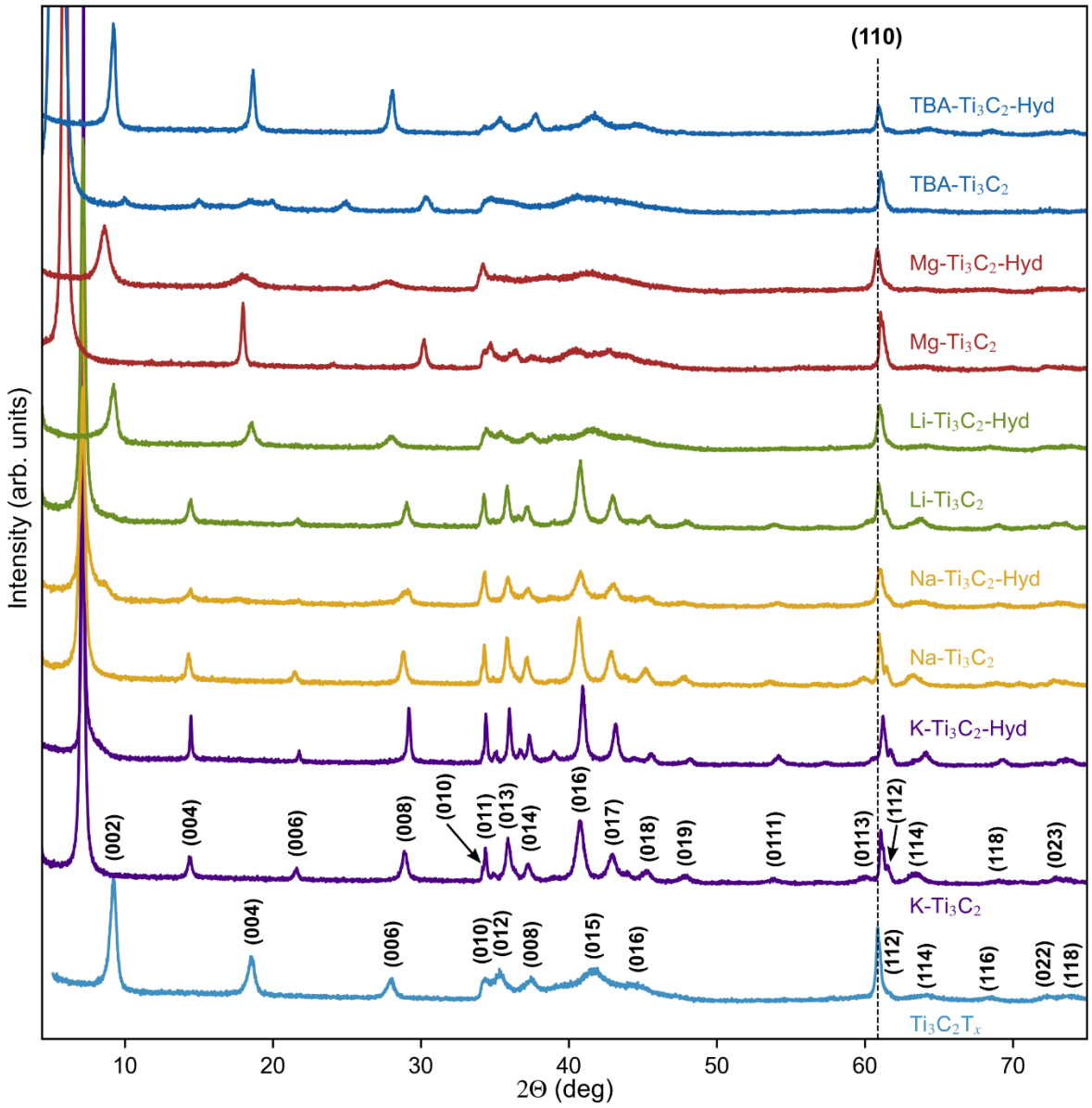

Figure S16. The whole X-ray diffractograms presented in Figure 4a, showing $Ti_3C_2T_x$ *intercalated with various cations before and after hydrolysation at 300 ˚C. It demonstrates how the diffractograms change a lot depending on the intercalated ions present, where the* Na- *and* K-*intercalated MXene as well as the* Li-*intercalated one before hydrolysation shows sharper reflections, and thereby a higher ordering of the structure, compared to the other samples. The dashed line marks the location of the (110) reflection of the pristine* $Ti_3C_2T_x$ *and illustrates the shifts in this reflection upon intercalation and hydrolysation. There are no visible reflections related to any* TiO_2 *phases in any of these diffractograms, indicating insignificant oxidation taking place. The (002) reflections are truncated to enhance the visibility of the other reflections, and the marked (hkl) planes are obtained from the structureless Pawley fitting of the* $Ti_3C_2T_x$ *and* K-Ti_3C_2 *phases using the* $P6_3/mmc$ *space group.*

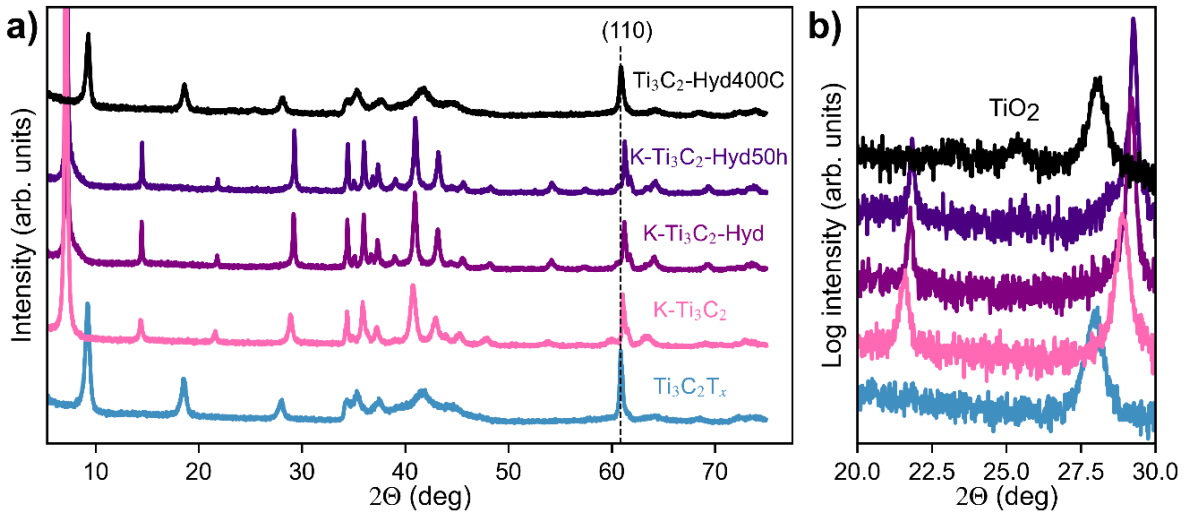

Figure S17. X-ray diffractogram of pristine $Ti_3C_2T_x$ *and* $Ti_3C_2T_x$ *after* K*-intercalation and hydrolysation at 300 ˚C for 15 h and 50 h, where (a) shows the overview diffractograms while (b) shows logarithmic values of a smaller region. The full height of the (002) reflections are truncated for a better presentation of the other reflections. The dashed line at 60.7 degrees represents the position of the (110) reflection of the pristine* HF*-etched* $Ti_3C_2T_x$ *and illustrates significant shifts upon intercalation and hydrolysation, attributable to stacking changes. The Hyd400C diffractogram (black) is added as a reference to demonstrate no reflections from* TiO_2 *at 25.3 degrees for the K-intercalated samples, even after hydrolysation for 50 h.*

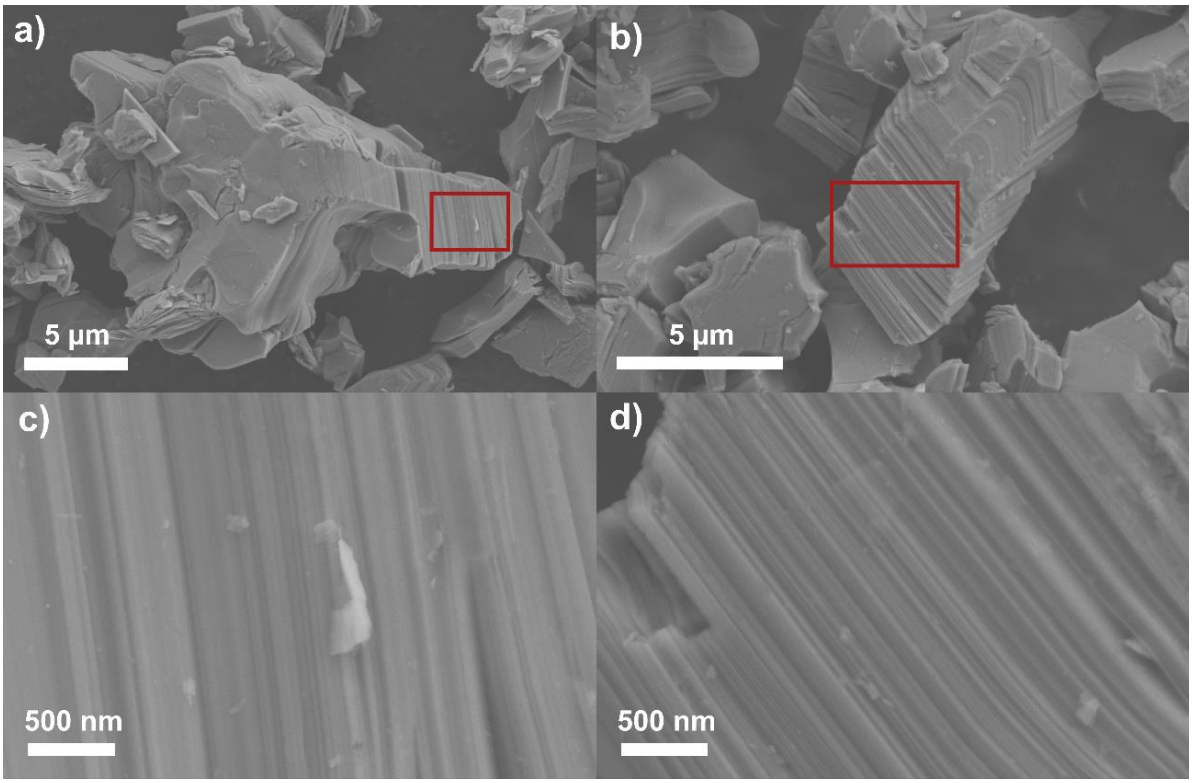

Figure S18. SEM micrographs of the K-Ti_3C_2 *(a,c) and* K-Ti_3C_2-Hyd *(b,d) samples at two different magnifications, where the red rectangles in a and b represent the areas depicted in c and d respectively. These micrographs show no obvious formation of* TiO_2 *nanoparticles on the edge surface after the intercalation of* K*-ions and the following hydrolysation at 300 ˚C.*

Table S3. The ionic radii, hydration enthalpy and solubility of respective fluorides for four cations (Mg^{2+}, Li^{+}, Na^{+} and K^{+}), demonstrating how the smaller ions bond stronger to F.

Cation	**Ionic radii (Å)**[6,7]	**Hydration Enthalpies $-\Delta H^{\circ}_{hyd}$ (kJ/mol)** [8]	**Solubility of fluorides in water (g/100 mL @ 25 ˚C)**[6]
Mg^{2+}	0.72	1921	0.013
Li^{+}	0.69	519	0.13
Na^{+}	1.02	409	4.1
K^{+}	1.38	322	102

References

[1] C. Ferrara, A. Gentile, S. Marchionna, I. Quinzeni, M. Fracchia, P. Ghigna, S. Pollastri, C. Ritter, G.M. Vanacore, R. Ruffo, The Missing Piece: The Structure of the Ti3C2TxMXene and Its Behavior as Negative Electrode in Sodium Ion Batteries, Nano Lett. 21 (2021) 8290–8297. https://doi.org/10.1021/ACS.NANOLETT.1C02809.

[2] Z. Li, L. Wang, D. Sun, Y. Zhang, B. Liu, Q. Hu, A. Zhou, Synthesis and thermal stability of two-dimensional carbide MXene Ti3C2, Mater. Sci. Eng. B Solid-State Mater. Adv. Technol. 191 (2015) 33–40. https://doi.org/10.1016/j.mseb.2014.10.009.

[3] P. Zheng, X. Zhang, M. Yan, Y. Ma, Y. Jiang, H. Li, The eruption of carbon chains in the oxidation of 2D Tin+1Cn (n = 1, 2, 3) MXenes, Appl. Surf. Sci. 550 (2021) 149310. https://doi.org/10.1016/J.APSUSC.2021.149310.

[4] C. Hou, J. Xie, H. Yang, S. Chen, H. Liu, Preparation of Cu 2 O@TiOF 2 /TiO 2 and its photocatalytic degradation of tetracycline hydrochloride wastewater, RSC Adv. 9 (2019) 37911–37918. https://doi.org/10.1039/C9RA07999H.

[5] M.M. Viana, V.F. Soares, N.D.S. Mohallem, Synthesis and characterization of TiO2 nanoparticles, Ceram. Int. 36 (2010) 2047–2053. https://doi.org/10.1016/J.CERAMINT.2010.04.006.

[6] A.G. Blackman, L.R. Gahan, G.H. Aylward, T.J.V. (Tristan J.V. Findlay, Aylward and Findlay's SI chemical data, Wiley, 2013.

[7] N. Shpigel, M.D. Levi, S. Sigalov, T.S. Mathis, Y. Gogotsi, D. Aurbach, Direct Assessment of Nanoconfined Water in 2D Ti 3 C 2 Electrode Interspaces by a Surface Acoustic Technique, J. Am. Chem. Soc. 140 (2018) 8910–8917. https://doi.org/10.1021/JACS.8B04862.

[8] D.W. Smith, Ionic hydration enthalpies, J. Chem. Educ. 54 (1977) 540–542. https://doi.org/10.1021/ED054P540.